Supplementary Information

Non-invasive monitoring of the growth of metal-organic frameworks (MOFs) *via* Raman spectroscopy

Magdalene W. S. Chong[a]*, Andrew J. Parrott[b]*, David J. Ashworth[cd], Ashleigh J. Fletcher[c], and Alison Nordon[ab]

[a] WestCHEM, Department of Pure and Applied Chemistry and EPSRC Future Continuous Manufacturing and Advanced Crystallisation Research Hub, University of Strathclyde, 99 George Street, Glasgow, G1 1RD, United Kingdom

[b] WestCHEM, Department of Pure and Applied Chemistry and Centre for Process Analytics and Control Technology (CPACT), University of Strathclyde, 295 Cathedral Street, Glasgow, G1 1XL, United Kingdom

[c] Department of Chemical and Process Engineering, James Weir Building, 75 Montrose Street, University of Strathclyde, Glasgow, G1 1XJ, United Kingdom

[d] Strathclyde Institute of Pharmacy & Biomedical Sciences (SIPBS), University of Strathclyde, 161 Cathedral Street, G4 0RE, Glasgow, United Kingdom

Additional Experimental Information

Small-scale preparation of F4_MIL-140A(Ce). Tetrafluoroterephthalic acid (30.4 mg, 0.128 mmol), deionised water (1.75 mL) and nitric acid (0.25 mL) were added to a vial. Ammonium cerium(IV) nitrate (68.4 mg, 0.125 mmol) and deionised water (0.50 mL) were added to another vial. The vials were heated to 60 °C to dissolve the solids. The yellow metal solution was added to the colourless ligand solution and the resulting yellow solution heated at 60 °C for *ca.* 1 hour. The pale yellow solid was isolated by vacuum filtration, washed with deionised water and then washed with acetone.

Small-scale preparation of F4_UiO-66(Ce). Tetrafluoroterephthalic acid (30.0 mg, 0.126 mmol), deionised water (0.90 mL), nitric acid (0.05 mL) and acetic acid (1.05 mL) were added to a vial. Ammonium cerium(IV) nitrate (68.2 mg, 0.125 mmol) and deionised water (0.50 mL) were added to another vial. The vials were heated to 60 °C to dissolve the solids. The yellow metal solution was added to the colourless ligand solution and the resulting turbid pale yellow mixture heated to 60 °C for *ca*. 1 hour. The off-white solid was isolated by vacuum filtration, washed with deionised water and then washed with acetone.

PhAT probe Raman measurements of components (Experiment 2). Raman spectra were acquired of the ligand and metal solutions in their respective Schott bottles by positioning the PhAT probe against the Schott bottle. After positioning the PhAT probe against the stirred tank reactor (STR), a Raman spectrum was acquired of the empty STR prior to addition of the ligand solution. These Raman spectra were acquired using an exposure time of 15 s and 4 accumulations. The Schott bottles and STR were wrapped in blackout material for spectral acquisition.

Experiment 6. In-line Raman spectra for Experiment 6 were acquired using an MR probe head fitted with a ¼ " immersion probe (Kaiser Optical Systems) fibre-coupled to an RXN2 Raman spectrometer (Kaiser Optical Systems). The 785 nm Invictus diode laser was operated at 350 mW at source. The spectrometer was operated using iC Raman (Mettler Toledo) software. In-line THz Raman spectra were acquired using the same THz Raman equipment as described for off-line spectra, except for a ½ " immersion optic (Kaiser Optical Systems) fitted instead of the non-contact optic.

Additional Raman data analysis details. Second derivative spectra were calculated using a 15-point filter width (software default) for the PhAT probe data and a 11-point filter width (ensuring filter width is less than narrowest peak width) for the MR probe and Tornado data. A second order polynomial was used in all cases.

Normalisation of the second derivative peak intensities of all of the components in Experiment 3 were against the minimum intensity measured at the wavelength corresponding to that component. In all cases, the normalisation accounts for the minimum value of a negative peak in the second derivative spectra corresponding to the highest concentration of the analyte.

Small-scale preparation of HKUST-1. Trimesic acid (111.1 mg, 0.529 mmol), *N*,*N*-dimethylformamide (DMF, 1 mL), ethanol (1 mL), and deionised water (1 mL) were added to a vial. Copper(II) nitrate trihydrate (232.8 mg, 1.001 mmol), DMF (1 mL), ethanol (1 mL), and deionised water (1 mL) were added to another vial. The vials were heated to 60 °C to dissolve the solids. The contents of both vials were mixed by transferring the solutions between the vials using a pipette and the mixture evenly redistributed back between the two vials. The blue solutions were heated at 60 °C for *ca*. 65 h. The dark blue solid was isolated by vacuum filtration and washed with ethanol/water (1:1 v/v).

Powder X-ray diffraction (PXRD). PXRD patterns of the products from the smaller scale (2 mL) screening experiments and for immediate analysis of the products from the larger scale (250 mL) experiments were collected on a D2 Phaser 2nd Gen (Bruker) benchtop diffractometer. The samples were lightly ground using a pestle and mortar and deposited onto a silicon zero background holder. PXRD patterns were collected over the 2θ range of 4 to 35 ° with a step size of 0.016 °, using Ni filtered Cu Kα irradiation and the X-ray source was operated at 30 kV and 10 mA. The samples were rotated at a rate of 15 rotations per minute during data collection.

High resolution PXRD patterns of the products from the larger scale (250 mL) experiments were collected using a D8 Discover (Bruker) diffractometer optimised for high-throughput transmission screen. The samples were lightly ground using a pestle and mortar and deposited onto Kapton film. PXRD patterns were collected over the 2θ range of 4 to 35 ° with a step size of 0.017 °, using Cu Kα irradiation and the X-ray tube was operated at 40 kV and 40 mA.

Reference PXRD patterns were calculated in Mercury (version 2020.3.0, CCDC) using a wavelength of 1.54056 Å.

Elemental analysis. Elemental analysis was performed on a CE440 CHN (Exeter Analytical) elemental analyser.

BET surface area. Nitrogen sorption measurements were carried out on an ASAP 2420 (Micromeritics) to determine the surface area of the MOFs. In each case, the MOF (*ca.* 0.4 g) was accurately weighed into a sample tube and degassed under vacuum at 110 °C for 2 h. This process removed any residual solvent or contaminants from the xerogel surface. Subsequently, low temperature (−196 °C, as maintained by the use of liquid nitrogen) nitrogen sorption analysis was performed, consisting of 40 adsorption points and 30 desorption points.

The nitrogen adsorption isotherms were analysed using the BET model[1] for unrestricted multilayer formation as expressed in Equation S1:

$$\frac{p}{(p^o - p)} = \frac{1}{n_m c} + \frac{(c-1)}{n_m c} \cdot \frac{p}{p^o} \qquad \text{(S1)}$$

where p^o is saturation vapour pressure; n is uptake, at pressure p, expressed as a molar quantity (mmol g^{-1}); n_m is complete monolayer coverage, expressed as a molar quantity (mmol g^{-1}); and c is a constant dimensionless quantity, related to the adsorption energy. Application of the BET equation has shown it to be linear only over the range p/p^o = 0.05 to 0.35.[1] The model fails at lower relative pressures due to adsorbent surface heterogeneity and at p/po > 0.35 where neglect of lateral interactions between neighbouring molecules and the process of capillary condensation produce deviations in the plot. The results are also subject to the recently recommended improvements to the BET model, which accounts for differences in the various pore size distributions in analysed materials.[2]

For samples exhibiting microporous character, a modification of the BET equation is required, and the range of relative pressures is amended on the basis of two criteria:[2]
(a) c must always be positive implying that any negative intercept on the BET plot indicates that one is outside the valid range of the BET equation.
(b) Application of the BET equation must be limited to the range where the term $V(1-p/p^o)$ continuously increases with p/p^o.
The resulting relative pressure range is then used to analyse the data as per the BET method outlined above.

Table S1 Experimental information for large-scale reactions. H_2L is tetrafluoroterephthalic acid, M is ammonium cerium(IV) nitrate Calculated CHN values and reported surface areas from reference 3.

Experiment number	System, conditions	Quantities	Spectral acquisition details	Mass solid collected / g	CHN / %		Surface area / $m^2\ g^{-1}$	
					Calculated	Found	Experimental	Reported
1	F4_MIL-140A(Ce), 60 °C	H_2L: 2.98 g, 12.5 mmol M: 6.85 g, 12.5 mmol	15 s exposure, 4 accumulations, 150 s intervals	2.70	C 23.4, H 0.49.	C 22.45, H 0.56.	13	320
2	F4_MIL-140A(Ce), 50 °C	H_2L: 2.98 g, 12.5 mmol M: 6.85 g, 12.5 mmol	30 s exposure, 4 accumulations, 270 s intervals	4.10	C 23.4, H 0.49.	C 22.64, H 0.54.	293	320
3	F4_UiO-66(Ce), 60 °C	H_2L: 2.98 g, 12.5 mmol M: 6.85 g, 12.5 mmol	15 s exposure, 4 accumulations, 150 s intervals	4.78	C 22.6, H 1.57.	C 19.93, H 0.52.	870	641
4	F4_MIL-140A(Ce), 60 °C	H_2L: 2.98 g, 12.5 mmol M: 6.85 g, 12.5 mmol	**PhAT:** 15 s exposure, 4 accumulations, 70 s interval **Hudson:** 2.5 s exposure, 4 accumulations, as fast as possible	4.39	C 23.4, H 0.49.	C 22.69, H 0.51.	61	320
5	F4_MIL-140A(Ce), 60 °C	H_2L: 2.98 g, 12.5 mmol M: 6.85 g, 12.5 mmol	**PhAT:** 15 s exposure, 4 accumulations, 70 s interval **Hudson:** 4.2 s exposure, 4 accumulations, as fast as possible	3.27	C 23.4, H 0.49.	C 23.36, H 0.58.	303	320
6	F4_MIL-140A(Ce), 60 °C	H_2L: 3.09 g, 13.0 mmol M: 6.90 g, 12.6 mmol	15 s exposure, 4 accumulations, 150 s intervals	0.89	C 23.4, H 0.49.	C 23.17, H 0.51.	316	320

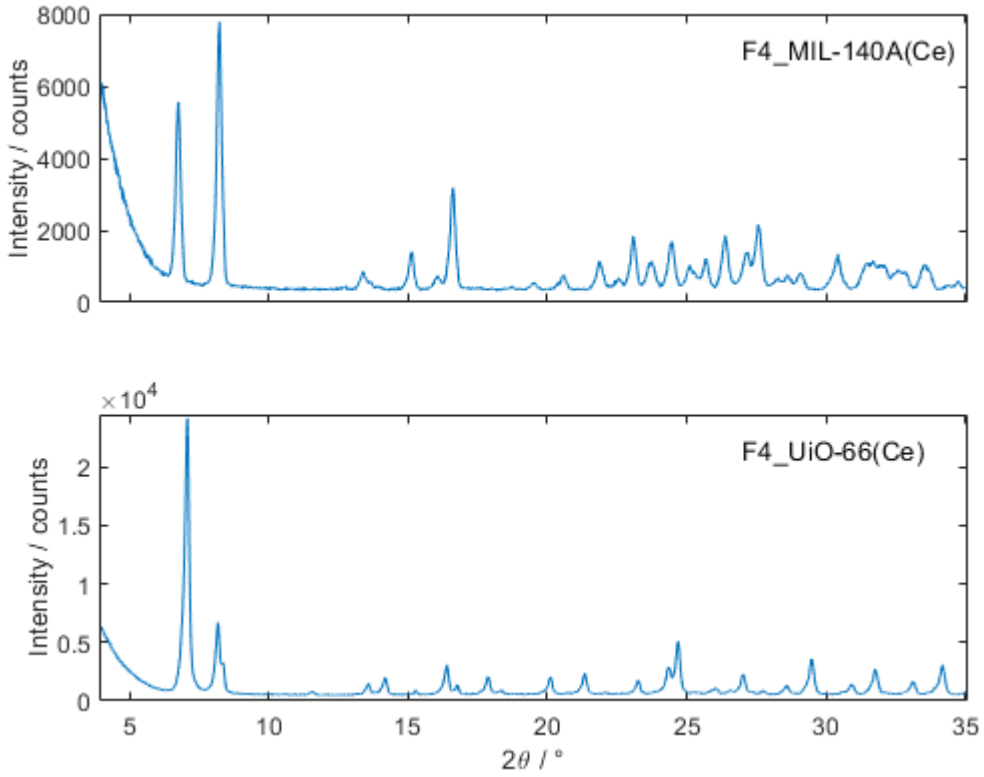

Figure S1 PXRD patterns of products from the small-scale preparations of the Ce MOFs.

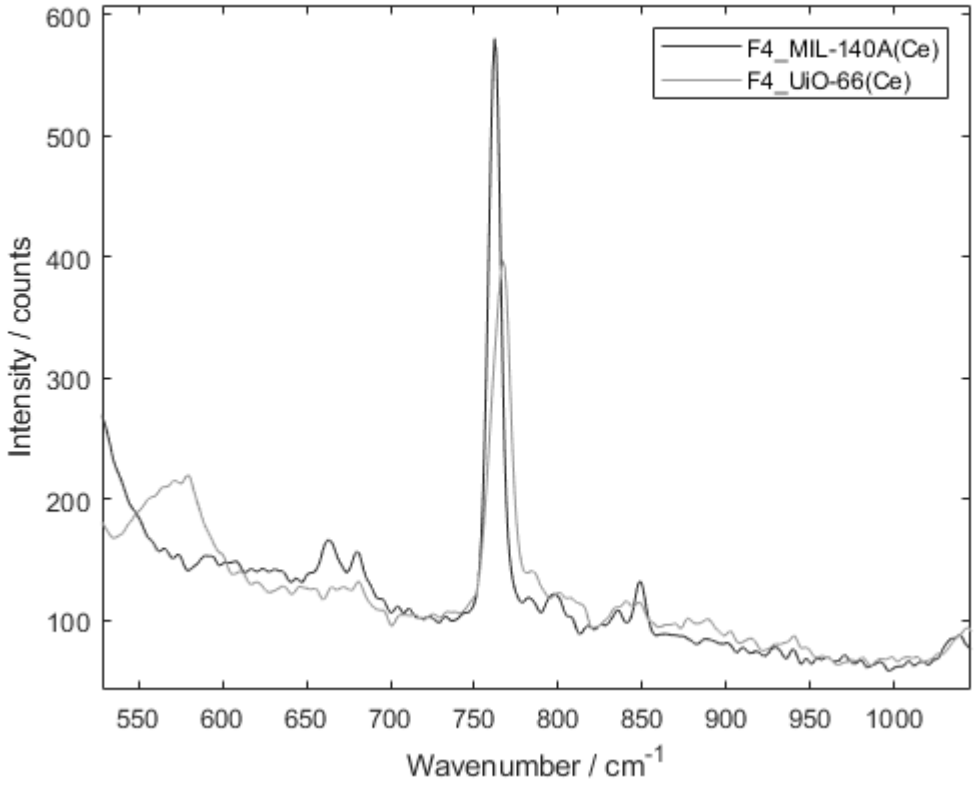

Figure S2 Different peaks observed at 762 and 768 cm^{-1} in the Raman spectra of F4_MIL-140A(Ce) and F4_UiO-66(Ce), respectively.

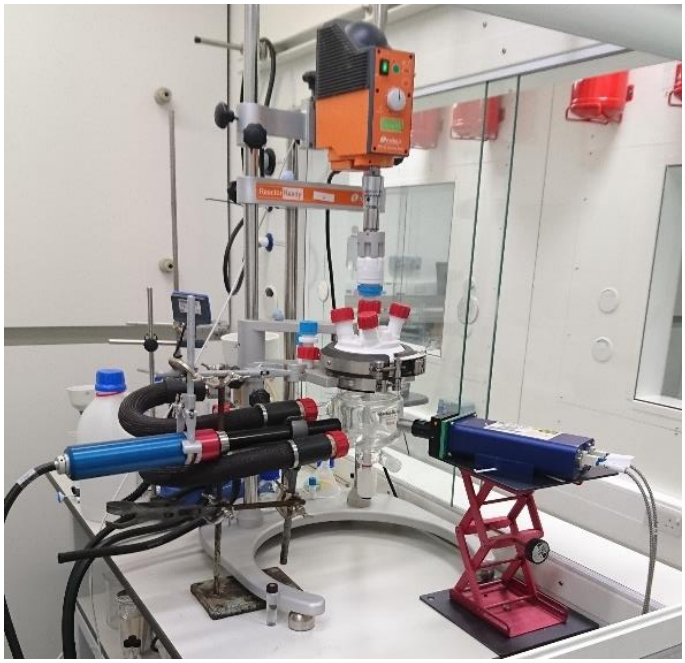

Figure S3 Photograph of setup for Experiment 1, showing 250 mL STR with non-invasive Raman and THz Raman monitoring.

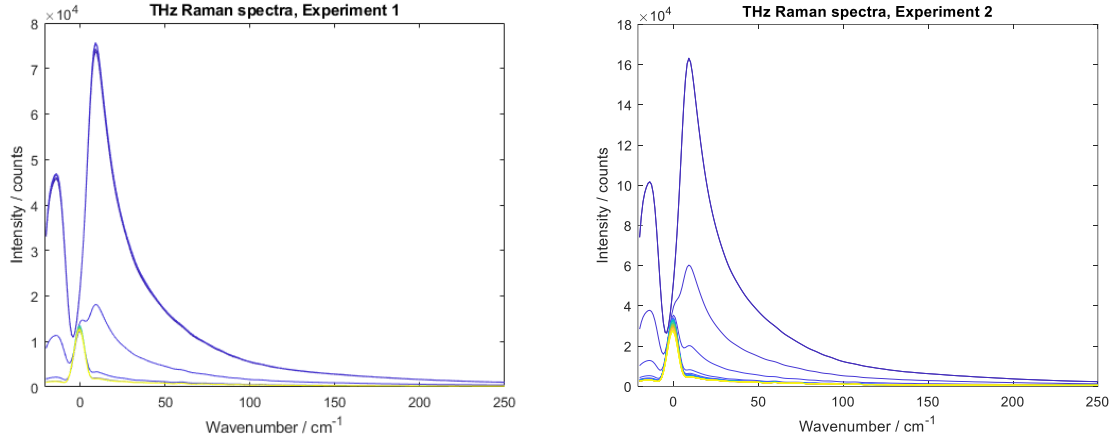

Figure S4 THz Raman spectra from non-invasive monitoring of Experiments 1 and 2.

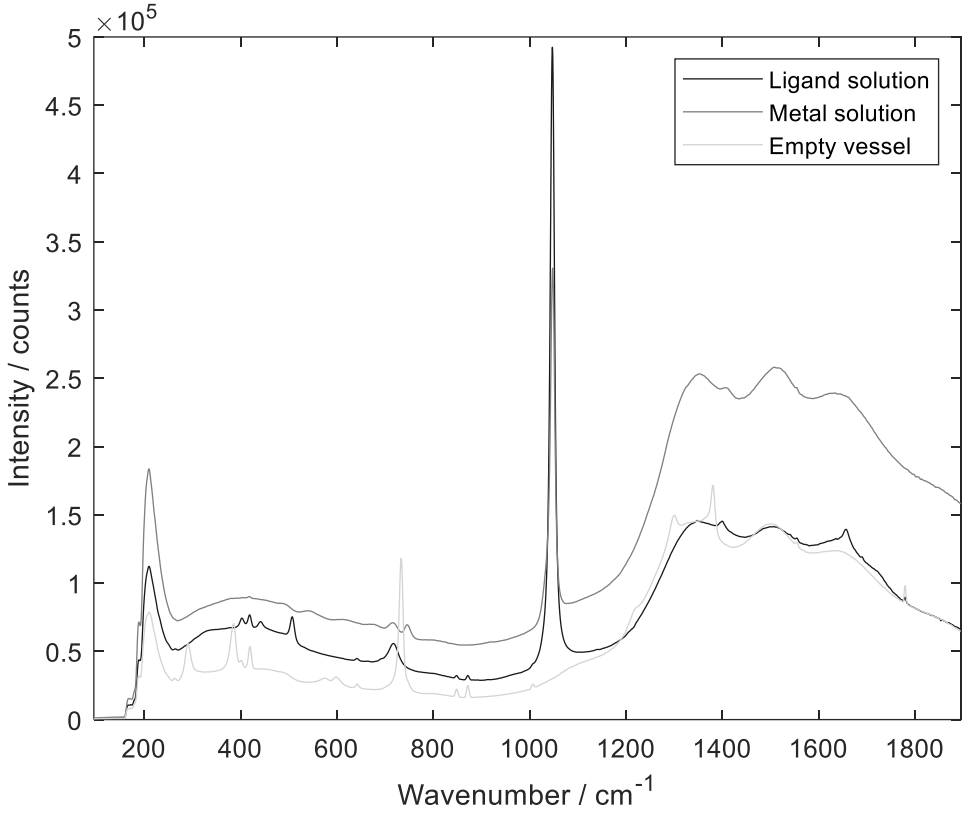

Figure S5 Raman spectra of the ligand solution, metal solution, and empty vessel (with stirrer in place) prior to addition of the solutions for Experiment 2. For the empty vessel, peaks arising from the polytetrafluoroethylene (PTFE)[4] stirrer are observed. Some common peaks (419, 642, 848, 872 cm^{-1}) observed for the metal solution and empty vessel are from room lights and do not interfere with the selected peaks of interest arising from tetrafluoroterephthalic acid, nitric acid, and F4_MIL-140A(Ce).

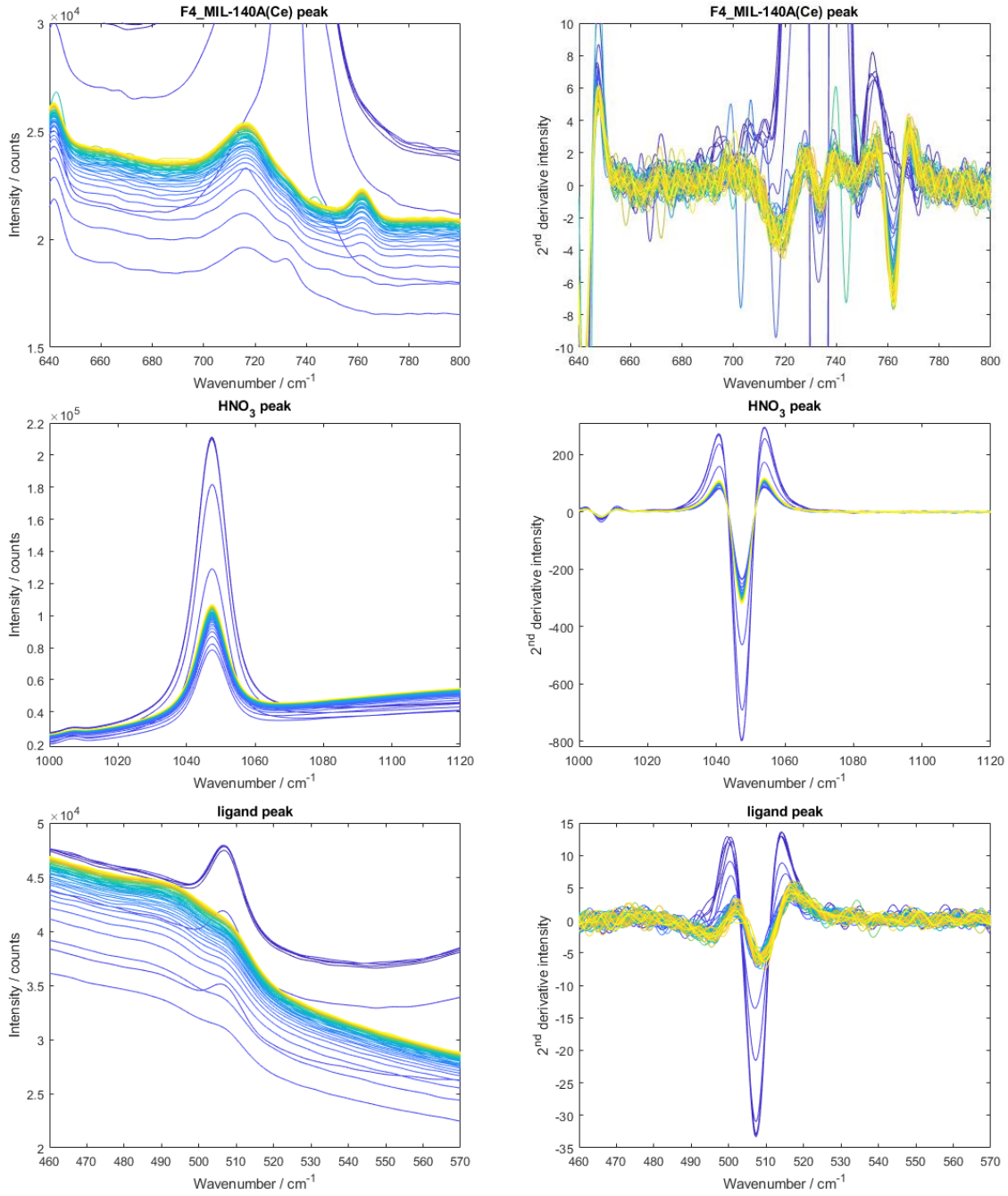

Figure S6 Raman spectra from PhAT probe monitoring of Experiment 1: (left) spectra as acquired and (right) second derivative spectra focussing on the peaks arising from (top) F4_MIL-140A(Ce), (middle) nitric acid and (bottom) tetrafluoroterephthalic acid ligand source in solution. The colour scheme goes from blue to yellow with reaction progress.

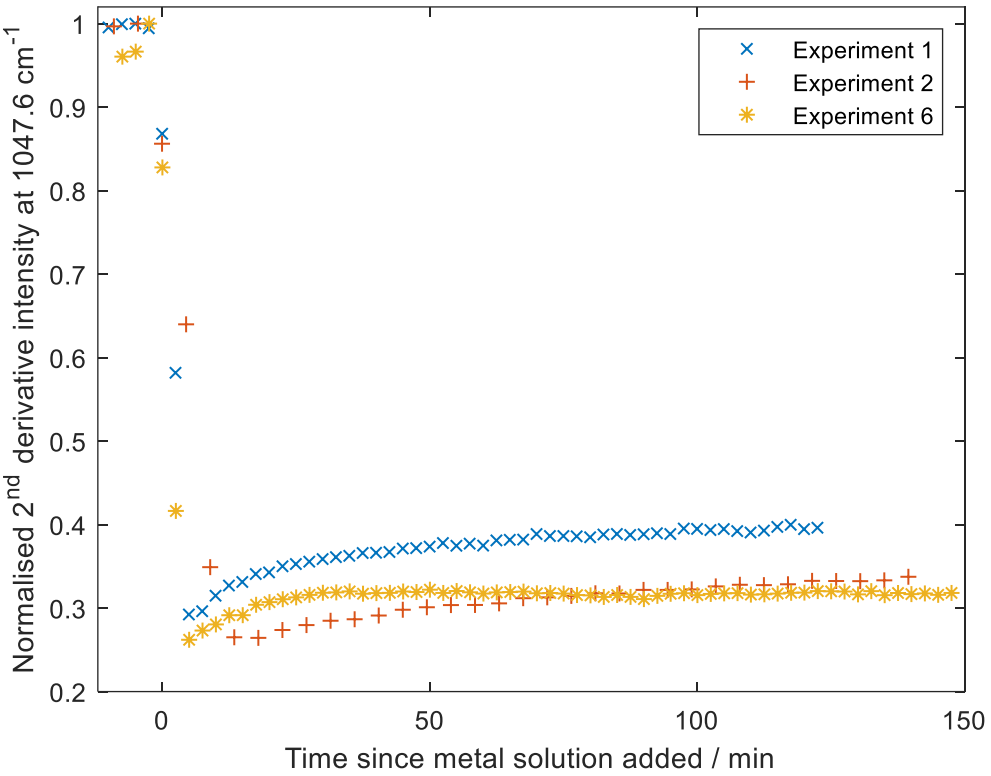

Figure S7 Normalised intensity of the second derivative nitric acid peak at 1047.6 cm^{-1} with reaction progress for Experiments 1, 2, and 6. NB. 1 corresponds to the highest concentration.

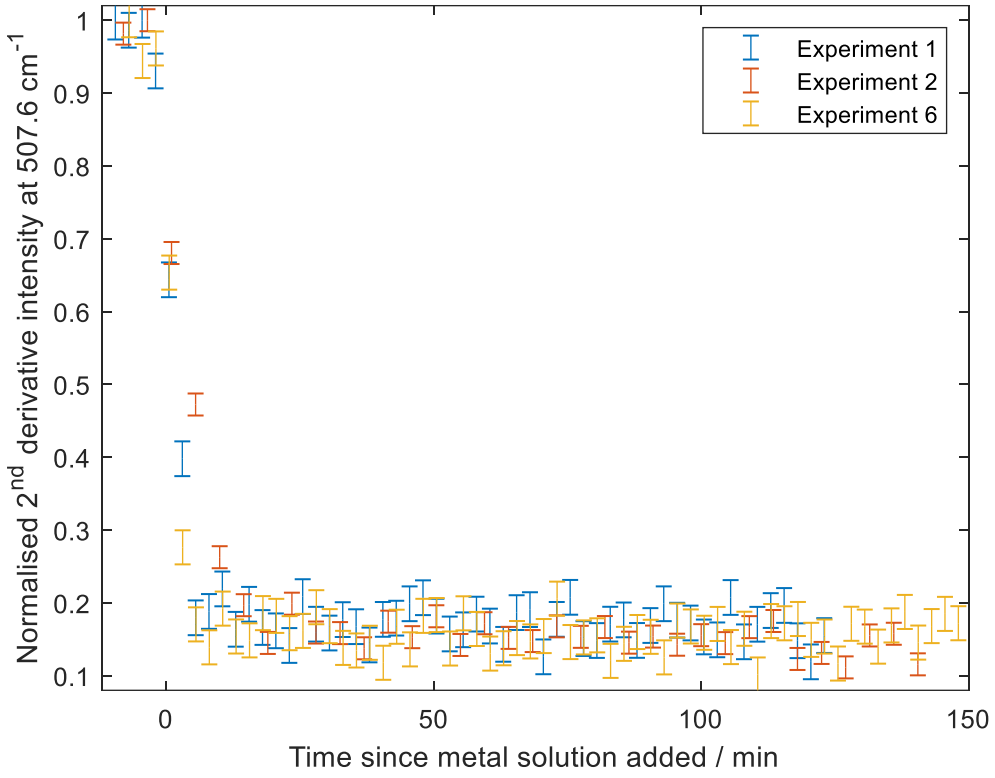

Figure S8 Normalised intensity of the second derivative ligand solution peak at 507.6 cm^{-1} with reaction progress for Experiments 1, 2, and 6. The error bars for each experiment correspond to the mean standard deviation over the wavenumber range 460.8 to 482.4 cm^{-1} of the second derivative spectra, in which variations are attributed to noise. NB. 1 corresponds to the highest concentration.

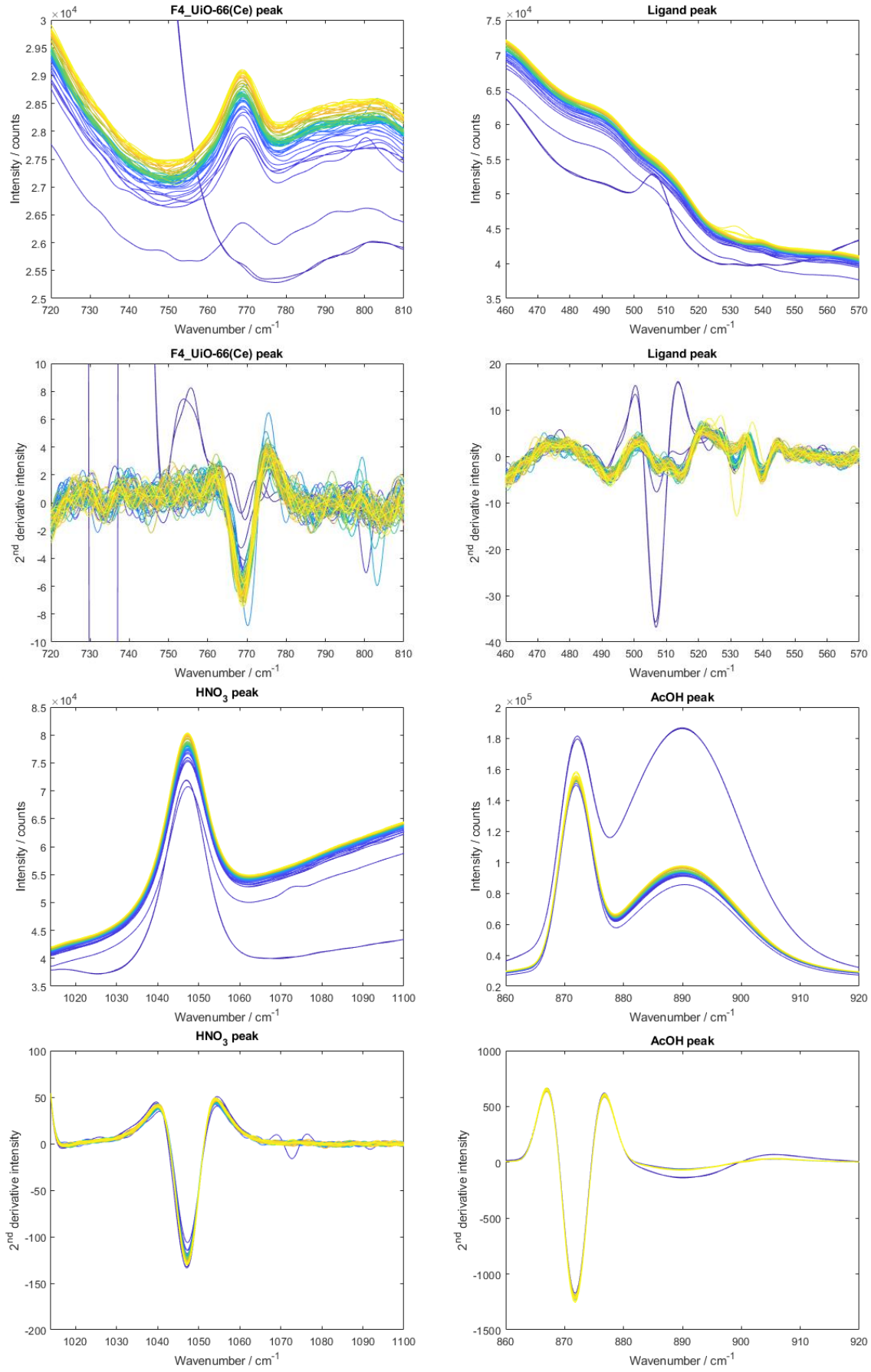

Figure S9 Features in the Raman spectra arising from the chemical components in Experiment 3.

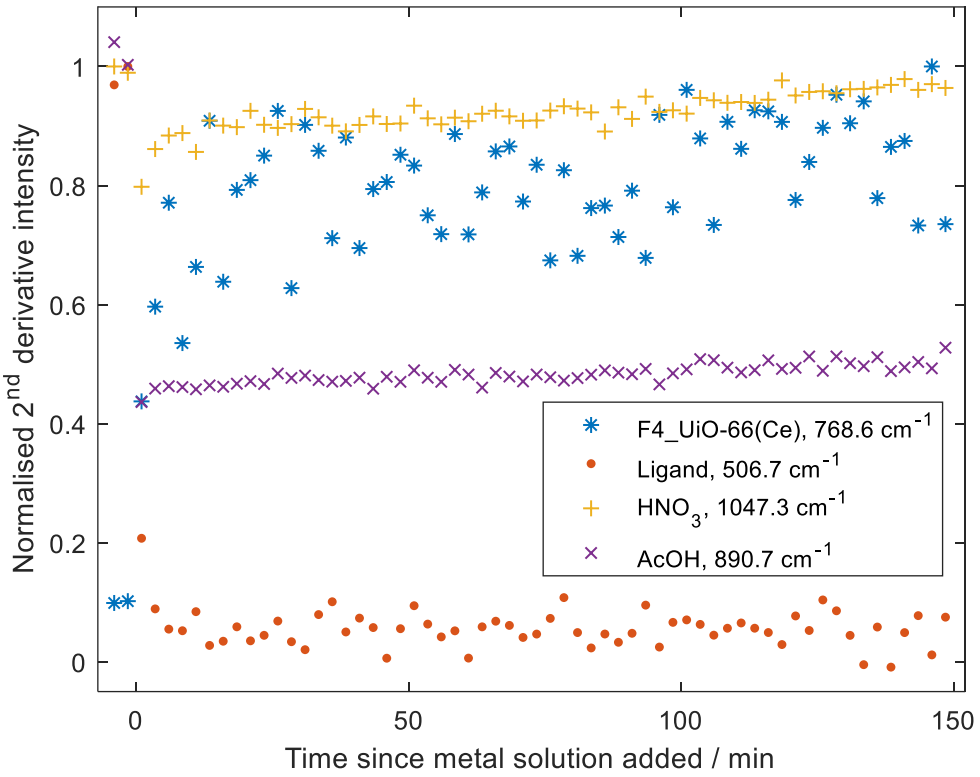

Figure S10 Normalised intensity of second derivative peaks corresponding to different components from non-invasive Raman monitoring of the synthesis of F4_UiO-66(Ce) in Experiment 3. NB. 1 corresponds to the highest concentration.

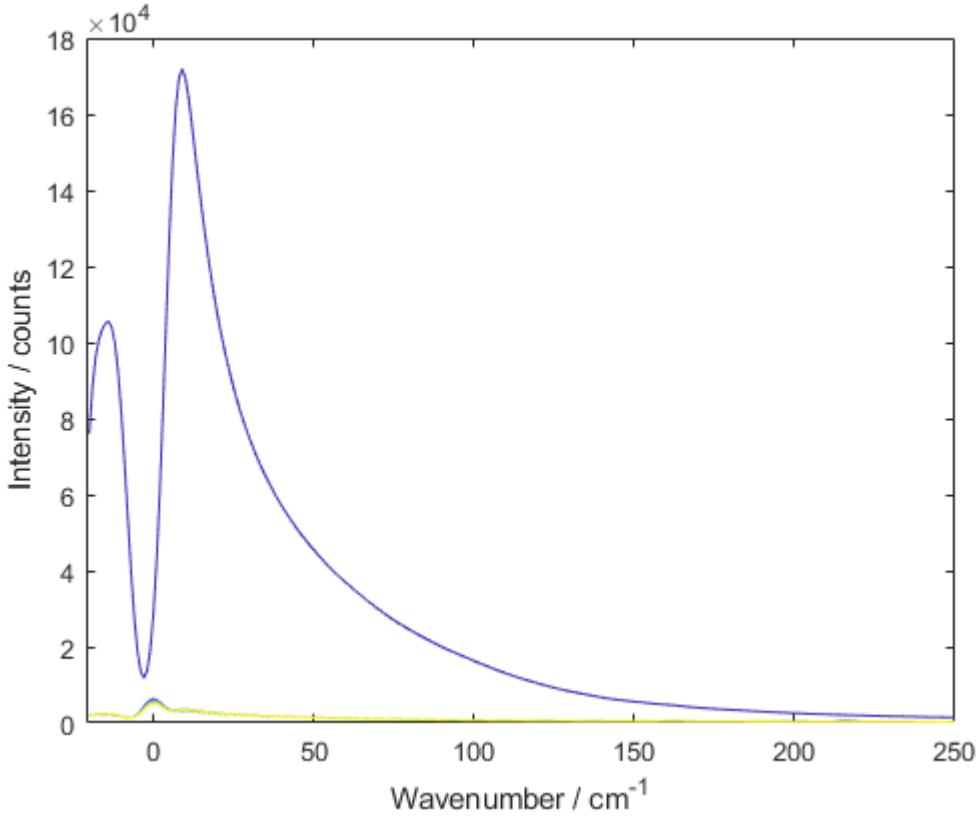

Figure S11 THz Raman spectra from non-invasive monitoring of Experiment 3.

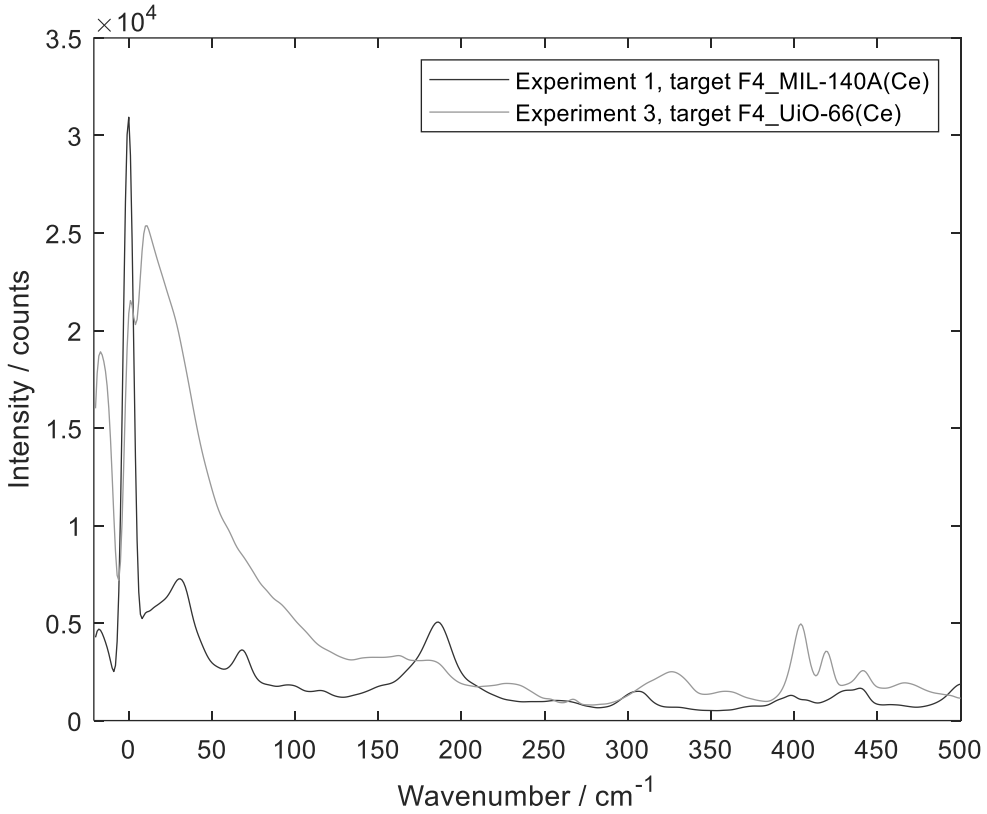

Figure S12 Off-line THz Raman spectra of the products obtained from Experiments 1 and 3.

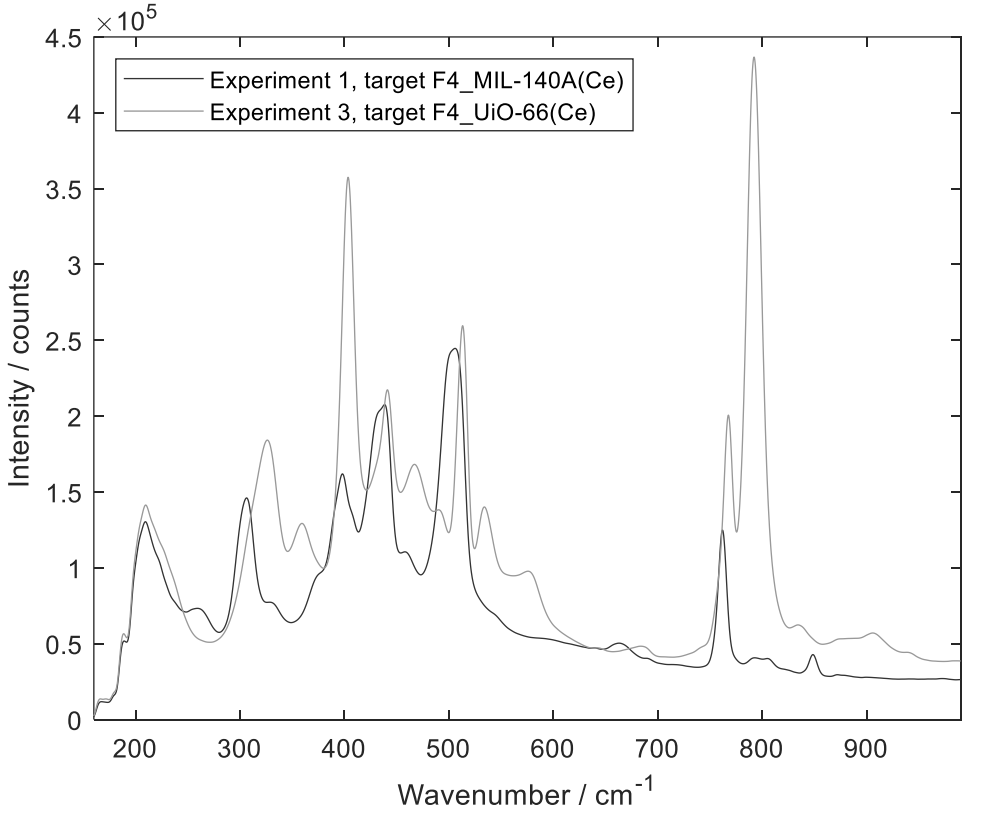

Figure S13 Off-line Raman spectra of the products obtained from Experiments 1 and 3, measured using the PhAT probe. The position of the CF peak is at 762 and 768 cm^{-1} for the product of Experiment 1 and 3, respectively.

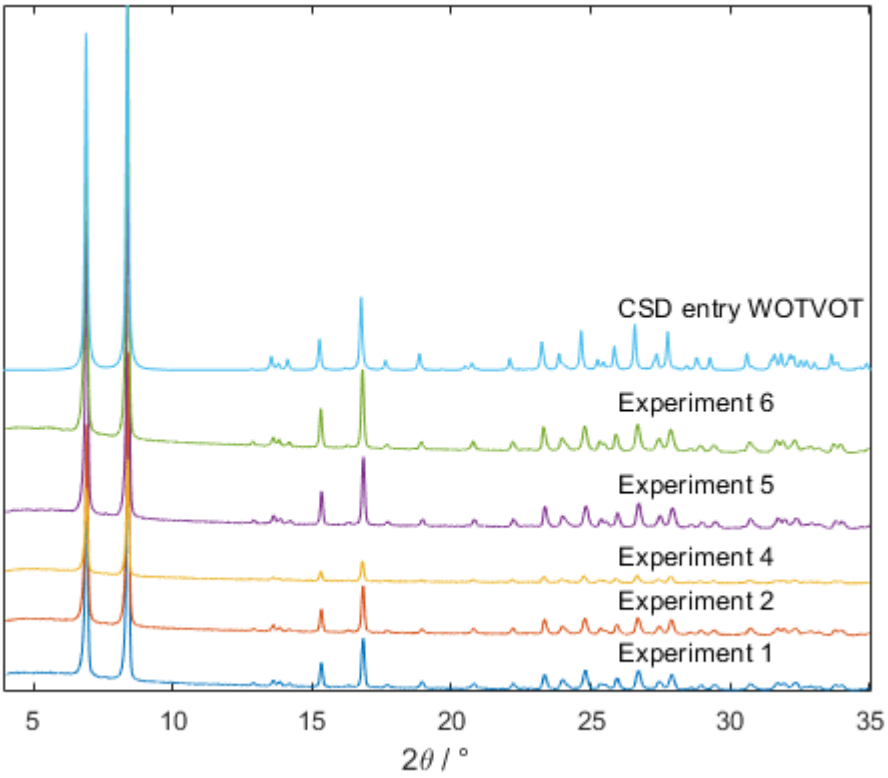

Figure S14 PXRD patterns of products obtained from Experiments 1, 2, 4, 5 and 6 overlaid from the simulated pattern from CSD entry WOTVOT (deposition number 1855704) for structure F4_MIL-140A(Ce).[3]

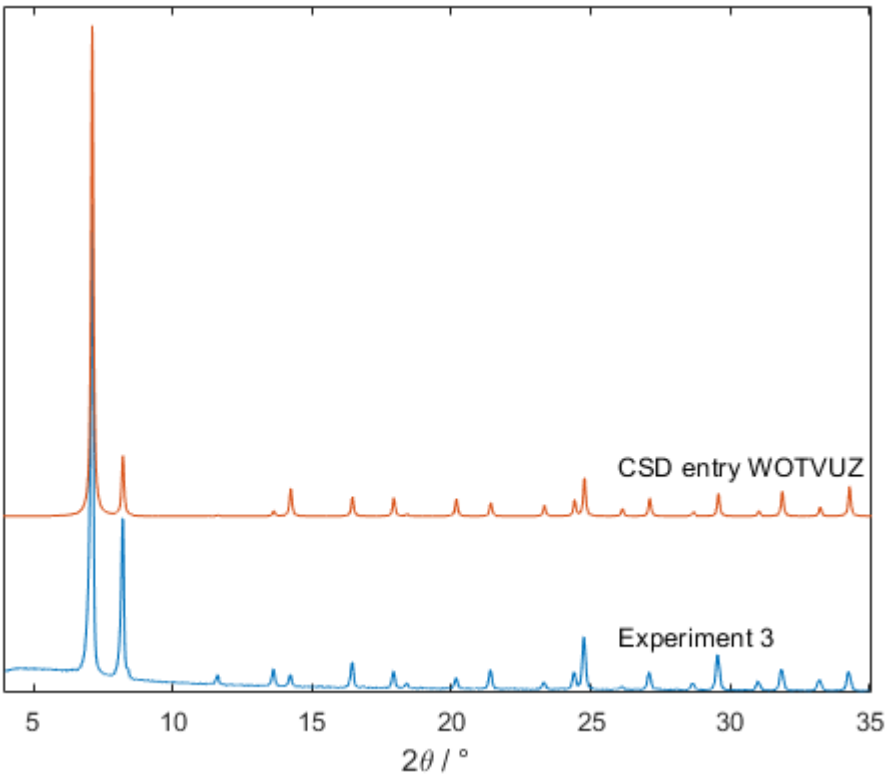

Figure S15 PXRD pattern of product obtained from Experiment 3 overlaid from the simulated pattern from CSD entry WOTVUZ (deposition number 1855705) for structure F4_UiO-66(Ce).[3]

Figure S16 Photograph of setup for Experiment 4, showing 250 mL STR with non-invasive Raman monitoring from the Kaiser PhAT probe and Tornado Hudson.

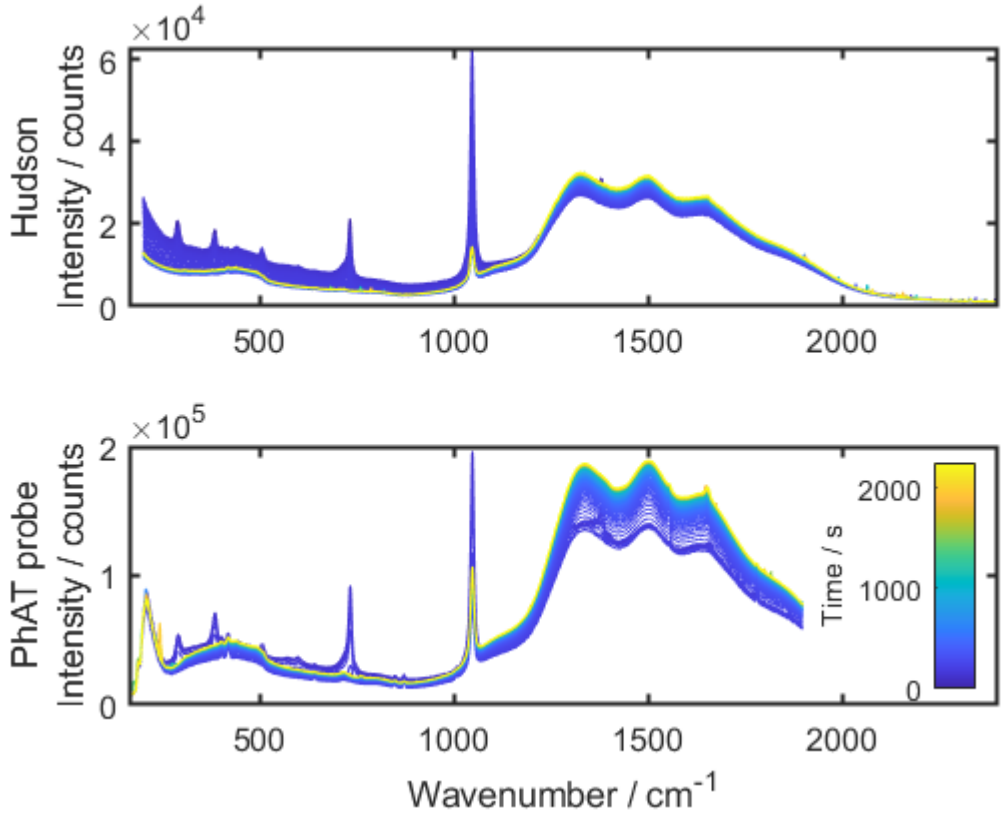

Figure S17 Raman spectra from non-invasive monitoring of Experiment 4 using (top) Tornado Hudson and (bottom) Kaiser PhAT probe. The colour scheme goes from blue to yellow with reaction progress.

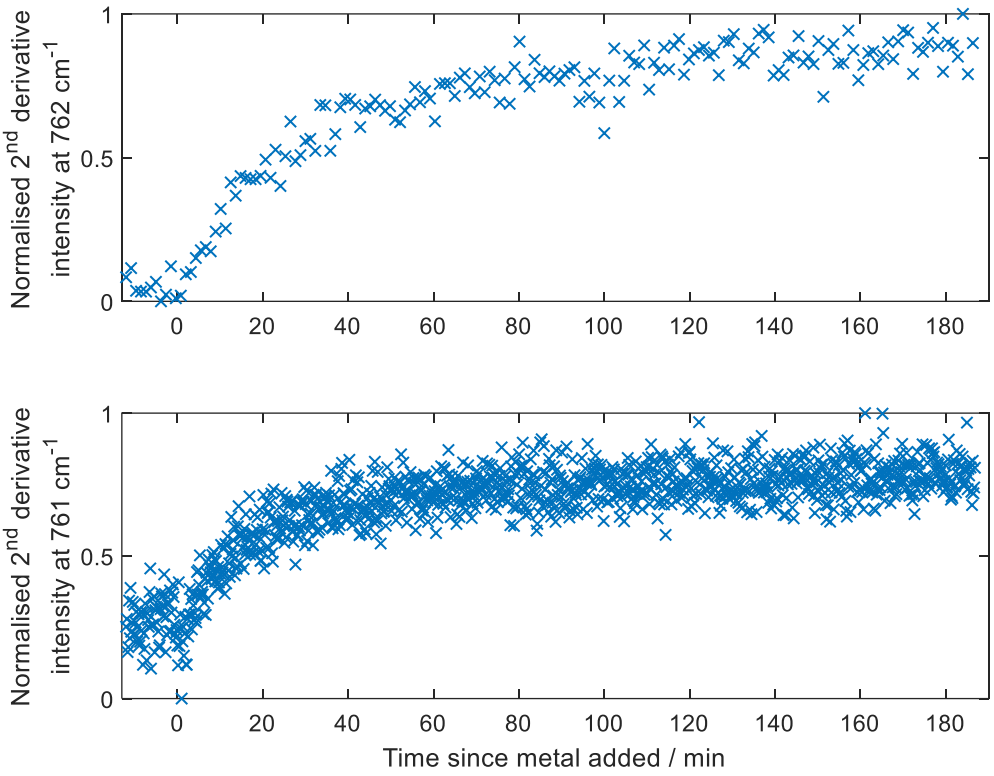

Figure S18 Normalised second derivative intensity of the F4_MIL-140A(Ce) peak from (top) PhAT probe and (bottom) Tornado Hudson monitoring of Experiment 4. NB. 1 corresponds to the highest concentration.

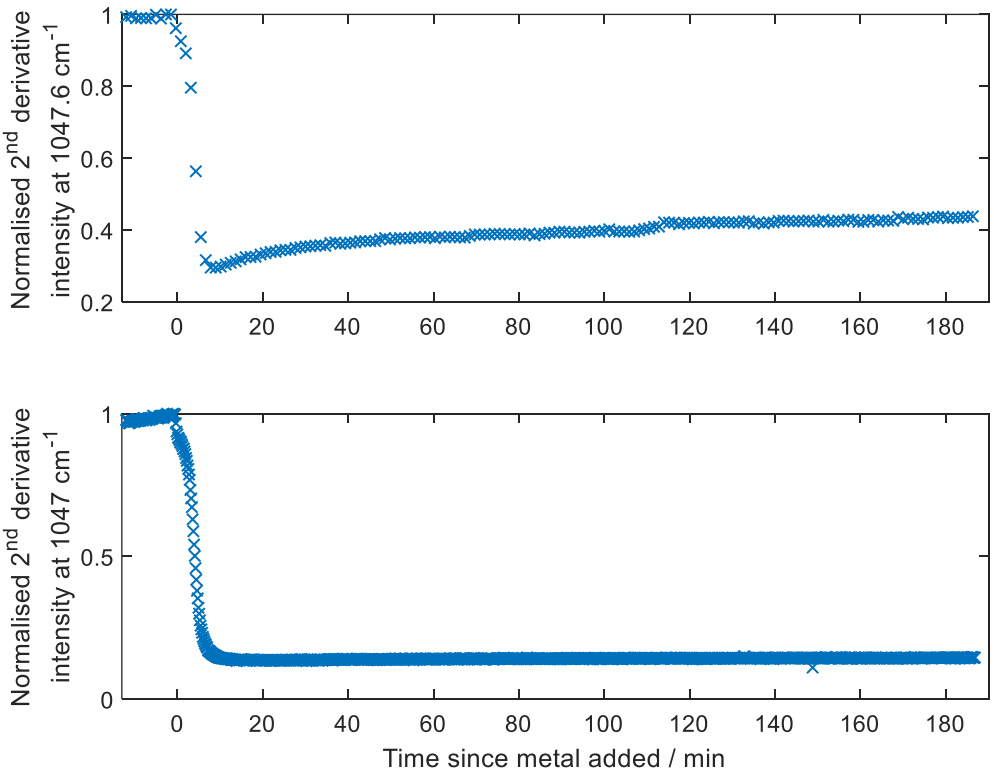

Figure S19 Normalised intensity of the second derivative nitric acid peak from (top) PhAT probe and (bottom) Tornado Hudson monitoring of Experiment 4. NB. 1 corresponds to the highest concentration.

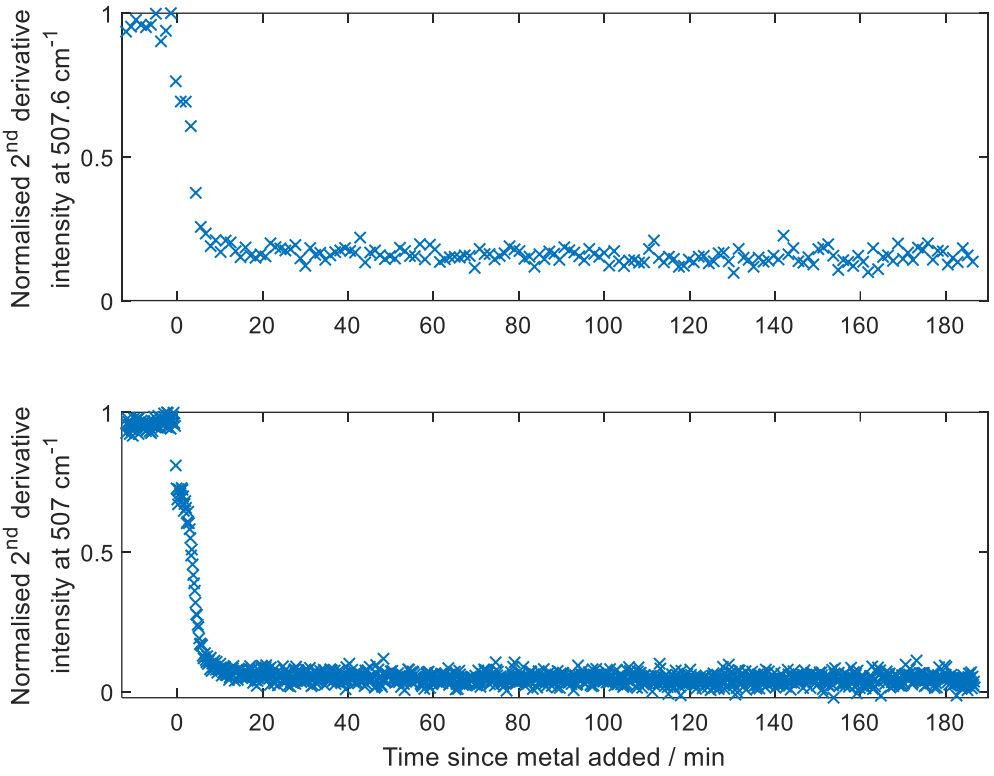

Figure S20 Normalised intensity of the second derivative ligand peak from (top) PhAT probe and (bottom) Tornado Hudson monitoring of Experiment 4. NB. 1 corresponds to the highest concentration.

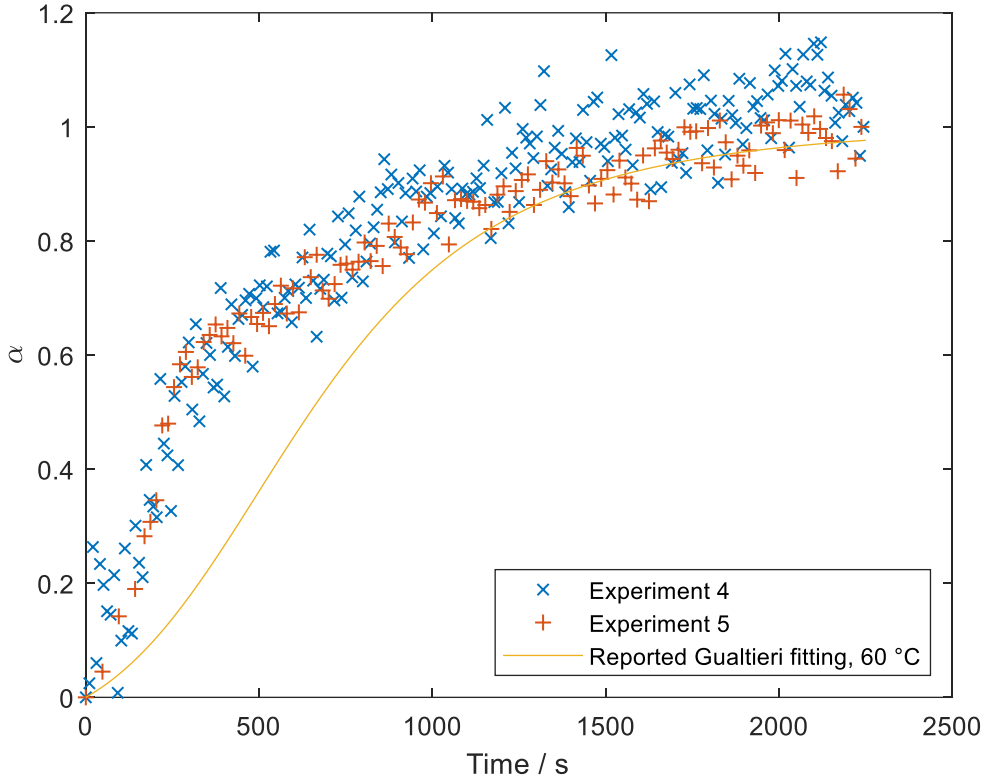

Figure S21 The extent of crystallisation, *α*, determined from the second derivative F4_MIL-140A(Ce) peak area at 762 cm^{-1} from non-invasive Raman monitoring *via* the Tornado Hudson in Experiments 4 and 5 overlaid with the reported Gualtieri fitting as a function of time for the formation of F4_MIL-140A(Ce) at 60 °C in the presence of 32 equivalents of nitric acid.[5]

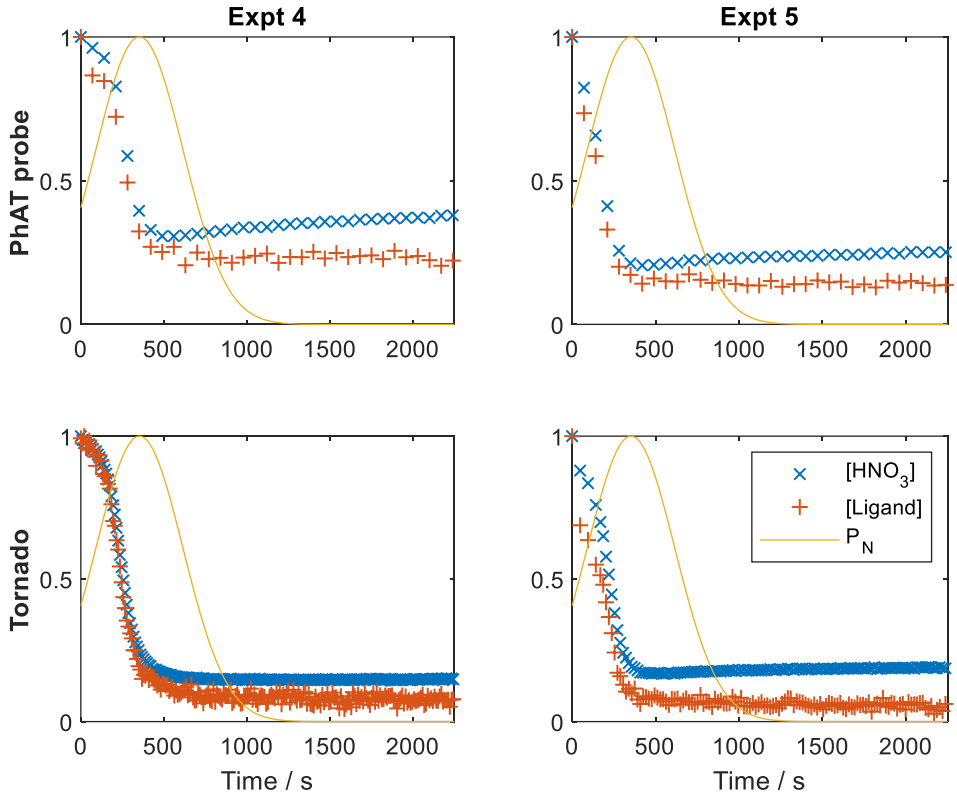

Figure S22 Change in normalised second derivative intensity of the nitric acid and ligand Raman peaks determined by non-invasive Raman monitoring of Experiments (left) 4 and (right) 5 using the (top) PhAT and (bottom) Hudson probes, overlaid against the reported probability of nucleation, P_N, for the formation of F4_MIL-140A(Ce) at 60 °C in the presence of 32 equivalents of nitric acid.[5] NB. For comparison, the bottom left figure is the same as Figure 6 in the paper.

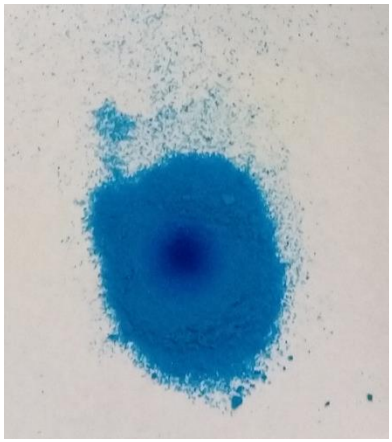

Figure S23 Photograph of HKUST-1 after acquisition of a Raman spectrum, there is a noticeably darker patch in the centre of the sample resulting from exposure to the 785 nm laser.

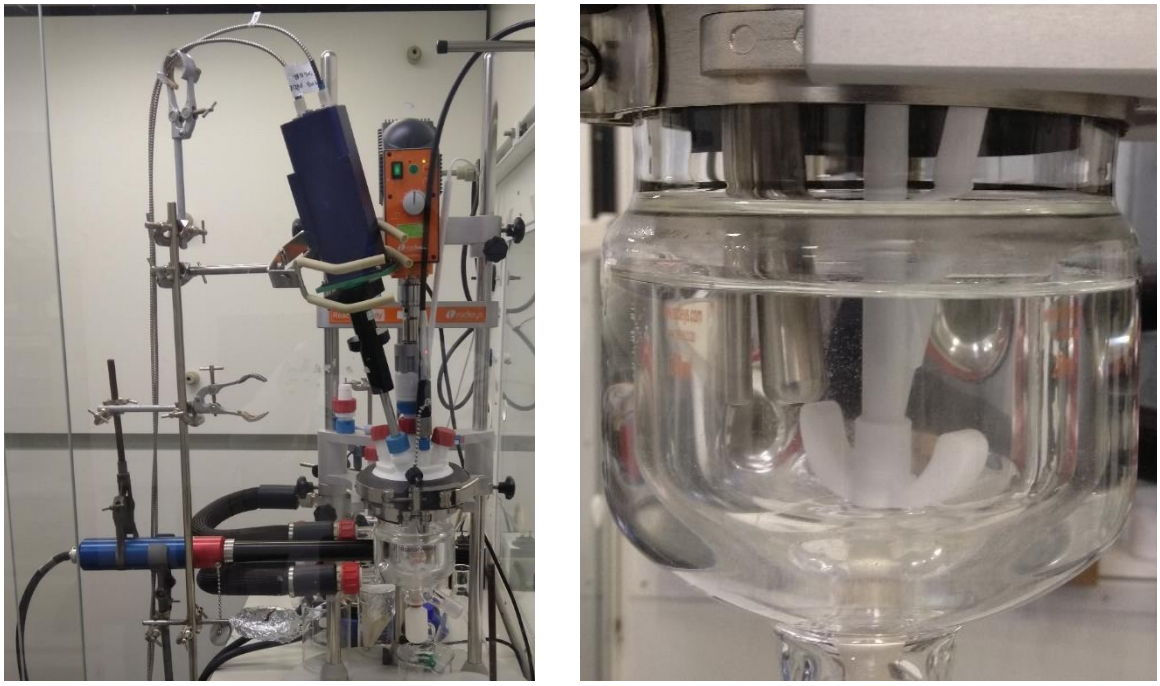

Figure S24 Photographs of (left) setup for Experiment 6, showing 250 mL STR with (right) invasive Raman and THz Raman probes.

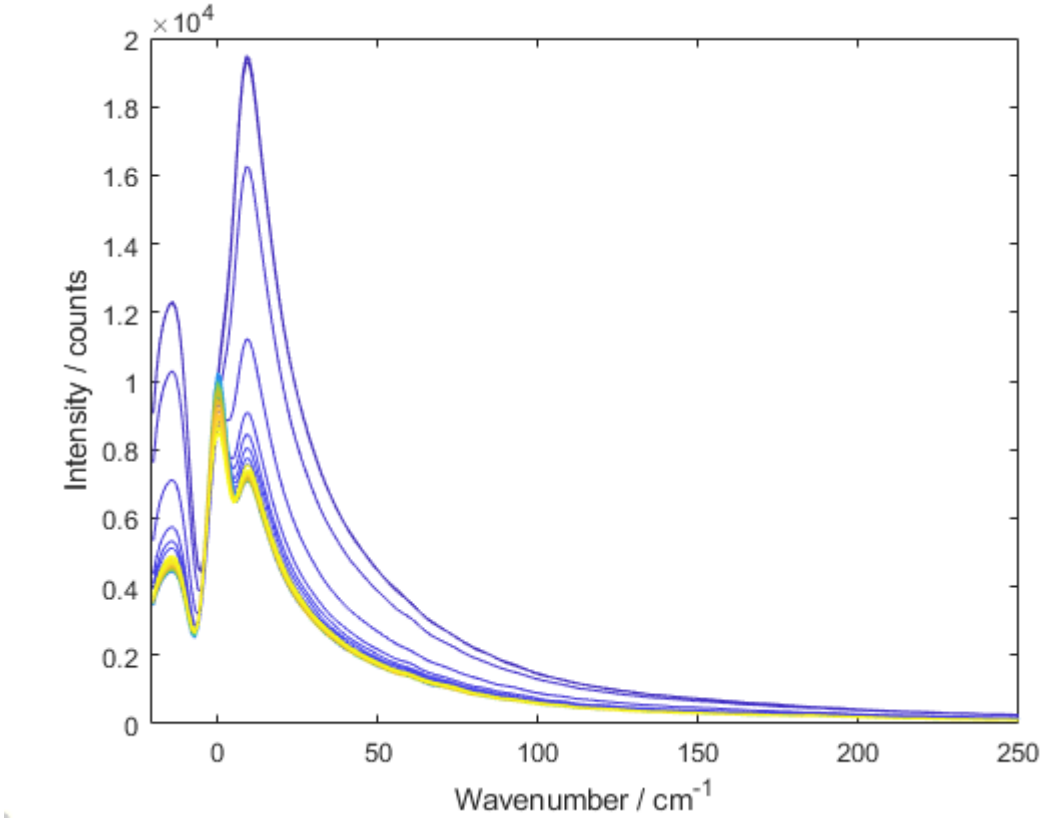

Figure S25 THz Raman spectra acquired using an immersion probe for monitoring of Experiment 6.

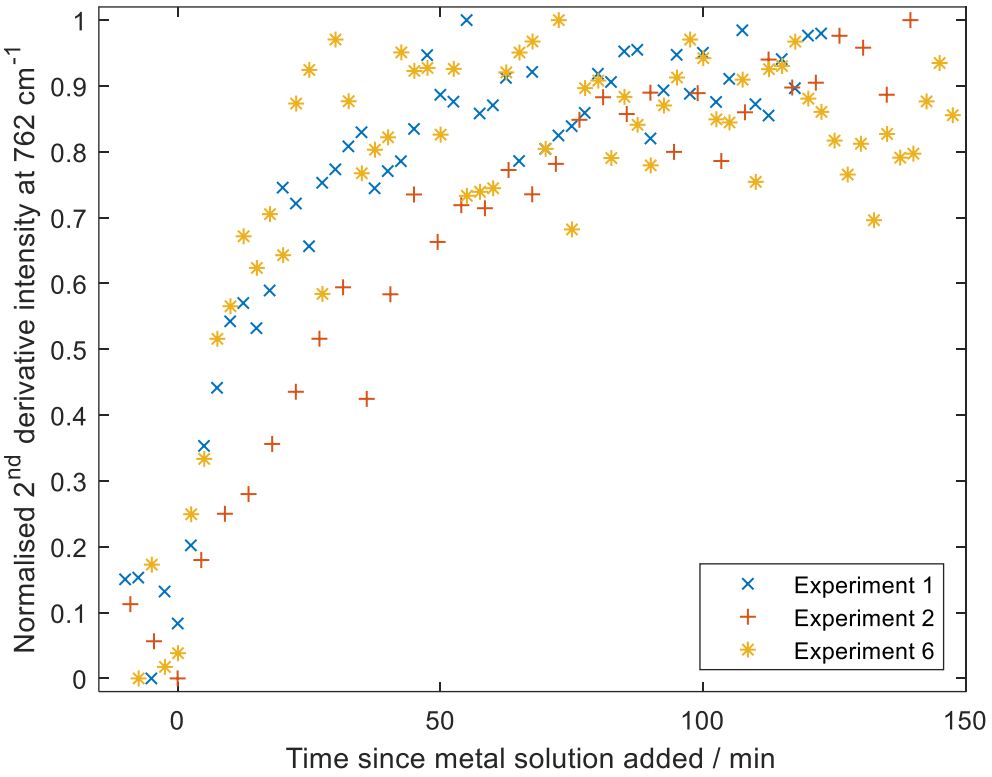

Figure S26 Normalised intensity of the second derivative F4_MIL-140A(Ce) Raman peak at 762 cm^{-1} with reaction progress for Experiments 1, 2, and 6. NB. 1 corresponds to the highest concentration.

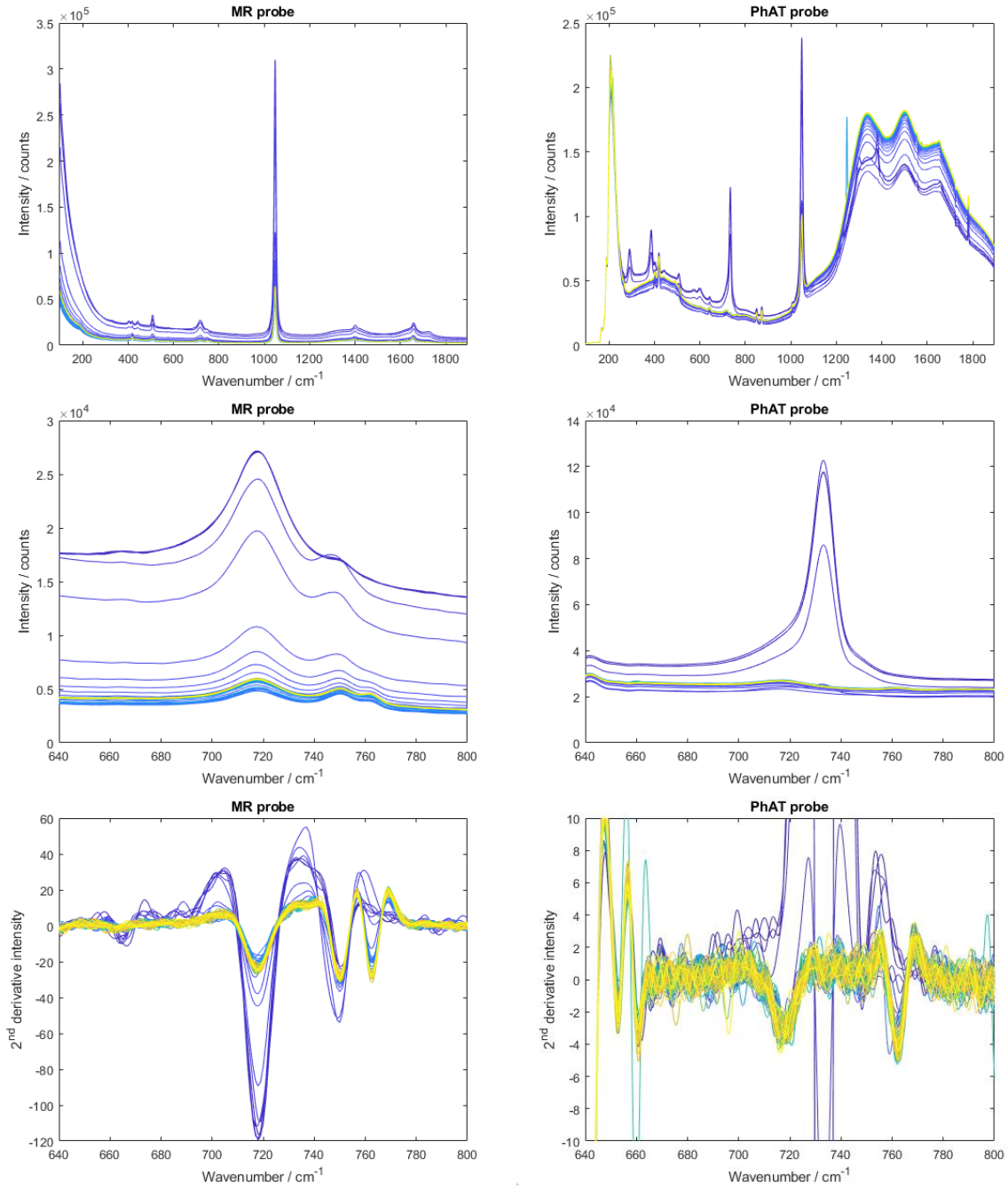

Figure S27 Raman spectra acquired using the (left) MR probe and (right) PhAT probe for Experiment 6: (top) full spectra, (middle) focussing on region around F4_MIL-140A(Ce) peak at 762 cm^{-1}, and (bottom) second derivative of region around F4_MIL-140A(Ce) peak at 762 cm^{-1}. The colour scheme goes from blue to yellow with reaction progress.

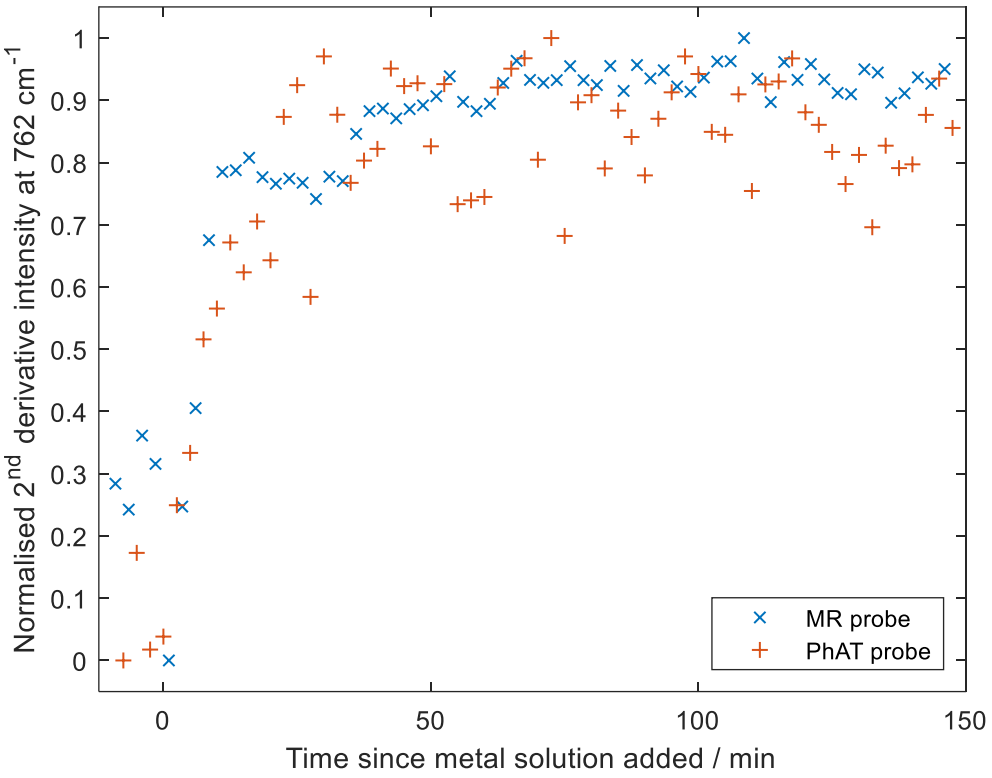

Figure S28 Change in intensity of the second derivative F4_MIL-140A(Ce) Raman peak at 762 cm^{-1} over the course of Experiment 6. NB. 1 corresponds to the highest concentration.

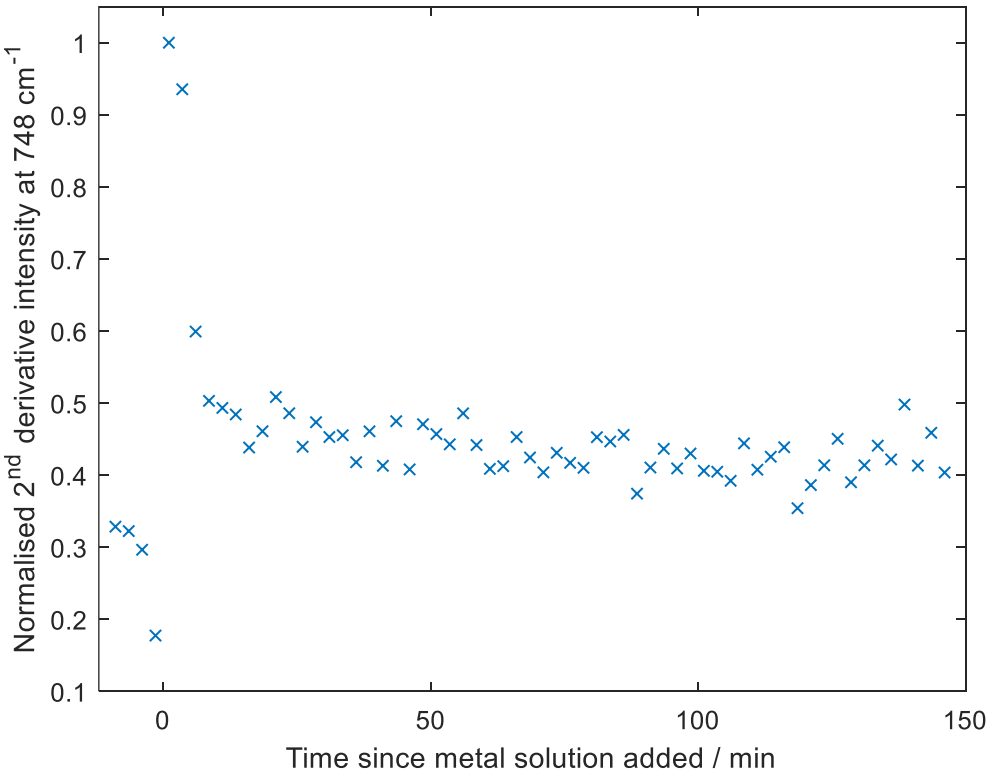

Figure S29 Change in intensity of the second derivative metal source Raman peak at 748 cm^{-1} from *in situ* monitoring of Experiment 6 *via* the MR probe. NB. 1 corresponds to the highest concentration.

References

1 S. Brunauer, P. H. Emmett and E. Teller, *J. Am. Chem. Soc.*, 1938, **60**, 309–319.

2 M. Thommes, K. Kaneko, A. V. Neimark, J. P. Olivier, F. Rodriguez-Reinoso, J. Rouquerol and K. S. W. Sing, *Pure Appl. Chem.*, 2015, **87**, 1051–1069.

3 R. D'Amato, A. Donnadio, M. Carta, C. Sangregorio, D. Tiana, R. Vivani, M. Taddei and F. Costantino, *ACS Sustain. Chem. Eng.*, 2019, **7**, 394–402.

4 J. L. Koenig, F. J. Boerio, I. J. L. Koenig and F. J. Boehio, *J. Chem. Phys.*, 1969, **50**, 2823–2829.

5 S. J. I. Shearan, J. Jacobsen, F. Costantino, R. D'Amato, D. Novikov, N. Stock, E. Andreoli and M. Taddei, *Chem. – Eur. J.*, 2021, **27**, 6579–6592.